The effects of annealing temperature on size, shape, structure and optical properties of synthesized zinc oxide nanoparticles by sol-gel methods

B. Bekele[*], L. T. Jule, A. Saka
Department of Physics, College of Natural and Computational Science, Dambi Dollo University, Ethiopia

Annealing affects zinc oxide nanoparticles (ZnONPs) in terms of size, structure, composition, shape, and optical properties. The aim of this study was to investigate the effects of annealing temperature on the particle size, structure, shape, chemical composition, and optical properties of synthesized ZnONPs by sol-gel method. The samples were characterized using X-Ray Diffraction (XRD), Scanning Electron Microscopy (SEM), Fourier Transform Infrared (FT-IR), UV/Vis spectroscopy, and Photoluminescence. From XRD result, the synthesized ZnO has pure phase hexagonal wurtzite structure. Particle size, diffraction intensity, lattice parameters, bond length and spacing distance increase with the increase in annealing temperature, while strain size and full width at half maxima is decreased. Spherical images of synthesized ZnONPs were detected from SEM images. FT-IR peaks appeared in the region of 400-500cm^{-1} indicated the successful synthesizes of ZnONPs. The optical absorption of ZnONPs measured at different annealing temperatures showed that red shift as the annealing temperature was increased. The energy band-gap of synthesized ZnONPs was increased as annealing temperature increases. The emission peaks of synthesized nanoparticles are independent of the temperature while its emission intensity depends on the temperature.

1. Introduction

Zinc oxide nanoparticles (ZnONPs) have unique physical and chemical properties, such as high chemical stability, high photo-stability, broad range of absorption radiation, high electrochemical coupling coefficient and multifunctional materials [1, 2]. It has wide energy band gap (3.37eV), large exciton binding energy (60meV), high thermal and mechanical stability [3]. Easy to synthesis, tunable energy band gap, controlled shape and size, low cost production and non-toxic are some excellent properties of Zinc oxide nanoparticles [4, 5]. The larger number of extrinsic and intrinsic defects in Zinc oxide structure is acting as emission centers. It emits light in many colors such as violet, blue, green, yellow and red [6, 7]. Because of these properties it has wide applications in wide area of energy generation and photo-catalysis [8, 9], medical science, industrial, cosmetics, and antibacterial [10, 11]. Several factors are reported in literatures which individually and collectively affect ZnONPs in terms of shape, sizes and optical properties. The various factors are precursors [12], concentrations [13], temperature [14], Stirring time [15], duration [16], surfactant concentrations [17], dopant concentration [11], solvent medium [18], pH of the reaction mixture [19], and source of light during synthesis [20]. Recently, researchers were used polymers to prepare a number of metal oxide nanoparticles where the polymer skeleton eventually limits the growth to a specific shape of the lattice [21, 22].

The recent XRD results of ZnONPs showed that, annealing temperature leads to an improvement in the crystallinity and an increment in crystal size, strain size, both Zn-O bond length and unit cell volume [23, 24].Additionally, ZnONPs were synthesized from zinc nitrate hexahydrate $(Zn(NO_3)_2.6H2O)$ and Polyvinyl Alcohol (PVA) under different annealing temperatures have an effect on particle sizes, structure, shape and optical properties of ZnONPs

---

[25, 26]. Increasing annealing temperature makes the intensity of the peaks to get sharpened and increased with increasing annealing temperature. Crystallinity and crystal size of zinc oxide nanoparticles were primarily increased as temperature increase. Similarly, peak intensity is mainly increased due to the increment of the crystallinity and crystal size. Therefore, annealing temperature influences the morphology and particle size of synthesized zinc oxide nanoparticles. In this research, the effects of annealing temperatures on morphology, structure, sizes, chemical composition and optical properties of ZnONPs were investigated by the sol-gel method. The method has much interest due to its chemical stability, low cost, reliability, gives relatively high purity, and homogeneous.

2. Materials and methods

2.1. Material used

Sodium hydroxide (NaOH) was used as chelating agents while zinc nitrate hexahydrate hydrate ($Zn(NO_3)_2.6H_2O$) were used as precursor chemical and both are purchased from Himedia, India: assay>99.2%.

2.2. Synthesis methods

ZnONPs were prepared by the soil-gel method according to the procedure developed in [27]. 5gm of Sodium hydroxide (NaOH) was dissolved in 50ml of double distilled water and stirred for 20min until a homogeneous white milk solution were obtained. In addition to this, 3gm of zinc nitrate hexahydrate ($Zn(NO3)_2.6H_2O$) was also dissolved in 3ml of double distilled water and stirred by a magnetic stirrer for 20min.Then, zinc nitrate hexahydrate($Zn(NO_3)_2.6H_2O$) solution was slowly added to sodium hydroxide solution (NaOH) drop by drop without touching the wall of the container at 70℃ under gentle magnetic stirrer for 2hr. The mixed solution should be stirred till the gel like substances are formed. The gel sample was allowed to dry in an oven at 140℃ for 10hrs. The sample was annealed in a muffle furnace (Model No: MC2-5/5/10-12, Biobase, Chaina) at the annealing temperature of 700℃ in open air for 8hrs.The same procedures were processed at annealing temperature of 800℃ and 900℃.

2.3. Characterization methods

The x-ray diffraction pattern of ZnONPs was analyzed using XPERTRO X-ray Diffractometer by generating Cu-Kα radiation (λ=0.154nm). It was used to analysis the crystal size of synthesized zinc oxide nanoparticles. It also operates at high voltages of 40KV and 30mA of current at room temperature and intensity were measured in range of $2\theta= 10°<2\theta <80°$. All the diffraction peaks of synthesized ZnONPs were well indexed to the wurtzite structure of ZnO (JCPDS card no. 36-1451). The average crystalline size of synthesized ZnONPs was calculated from the Debye Scherrer formula as follows [28]

$$D = \frac{0.89\lambda}{\beta cos\theta} \tag{1}$$

where the parameter λ, β, θ and D are X-ray wavelength, Bragg's diffraction angle, Full width at half maxima of the peak and average particle size respectively. The grain size(ε), lattice parameters 'a' and 'c' and the spacing distance d_{hkl} for the wurtzite structure of ZnO NPs can be calculated using the Equations (2), (3) and (4) [29-36].

$$\varepsilon = \frac{\beta}{4tan\theta} \tag{2}$$

$$a= \sqrt{\frac{1}{3}}\frac{\lambda}{Sin\theta} and c=\frac{\lambda}{Sin\theta} \tag{3}$$

$$d_{lkh} = \frac{ac}{2}\sqrt{\frac{3}{c^2(h^2+hk+k^2)+3\frac{(al)^2}{4}}} \tag{4}$$

The unit cell volume (V) and Zn-O bond length (L) are given by:-

$$V=0.866\,a^3c \text{ and} L=\frac{a^3}{3} + (\frac{1}{2} - z)^2c^2 \text{ where } Z = \frac{a^2}{3c^2} + \frac{1}{4} \text{ [32]} \tag{5}$$

The morphology of synthesized ZnONPs was characterized using Scanning Electron Microscope (Hitachi, H-7600). The optical absorption of the samples was measured by UV/Vis spectrophotometer (Perkin Elmer, Lambda 950) in the wavelength regions of 200-500 nm at 2 nm resolution. The band gap energy of ZnONPs is calculated using Equation (6).

$$E=\frac{hc}{\lambda} \tag{6}$$

where C= $3x10^8\frac{m}{s}$, and h = $6.626x10^{-34}$JS (Plank's constant [33].The vibrational spectra of synthesized ZnONPs were measured by FT-IR (Perkin Elmer 65) in the range of wave number from 400-4000cm^{-1}. The photoluminescence properties of ZnONPs were measured by Spectrofluorometer (Fluoromax-4, Spectrofluorometer) at room temperature with Xe-lamp as the excitation light source at a resolution of 1nm. The excitation and emission spectra were measured in the range of 380nm to 500nm.

3. Results and discussion

The XRD diffraction patterns of synthesized ZnONPs at annealing temperature of 700℃, 800℃ and 900℃ are shown in figure 3.1. All XRD diffraction patterns of ZnONPs are in good agreement with the hexagonal wurtzite structure (Hexagonal phase, space group P63mc) with lattice parameter a=b=3.249Å and c=5.206Å as reported in JCPDS card no. 36-1451[34]. Nine diffraction peaks were observed at 2θ =31. 72°, 34.44^o, 36.25^o, 47. 56^0,56. 67^0, 62.84^o, 66.47^o, 67.92^{o}and 69.10^{o}corresponding to (100), (002), (101), (102), (110), (103), (200), (112), and (201) of crystal planes respectively. The peak (101) is the most intense peak and shows a preferred growth plane. No impurity was observed in the diffraction peaks patterns; therefore, it confirmed the high purity of ZnO products. The intensity of diffraction peaks was increased with increasing the annealing temperature while the crystalline of ZnO NPs was increased. This may indicate that high annealing temperature provides sufficient energy to crystallize to orient in proper equilibrium sites and causes an increase in intensity [34, 35].
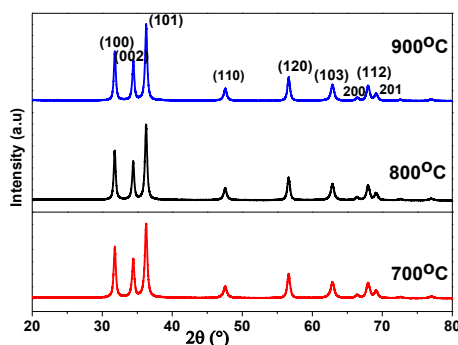
Fig. 3.1. XRD patterns of synthesized ZnONPs at annealing temperatures of 700℃, 800℃ and 900℃.

The average crystal sizes of synthesized ZnONPs were calculated by a Debye Scherrer formula using Equation (1) based on the full width at half-maximum (FWHM) of the peaks as shown in the Table 3.1. The average crystal sizes of ZnONPs annealed at temperature of 700℃, 800℃ and 900℃ are 33±20nm, 38±23nm and 48±33nm respectively. This result shows that, the average crystal sizes of ZnO NPs were increased as annealing temperature increased which is in good agreement with the result reported previously by [30-36]. In addition, Full Width at Half Maxima (FWHM) and average grain size of synthesized ZnONPs were decreased with increasing annealing temperature from 700℃ to 900℃. These results were corresponded with the crystallite sizes that obtained from the Debye Scherrer's equation (1). The small strain was observed in large crystalline whereas the small crystallite size that composed with small grain size induced the large strain [37].

Table 3.1. Full Width at Half Maxima (FWHM), average particle size and average strain value of ZnONPs at annealing temperature of 700℃, 800℃ and 900℃.

Annealing Temperature	FWHM (β)	Average particle Size(D)	Average strain value(ε)
700°C	0.04355	33±20nm	0.0148
800°C	0.03819	38±23nm	0.0130
900°C	0.03004	48±33nm	0.01024

The effects of annealing temperature on the lattice parameter of synthesized ZnONPs were calculated using equation (3) and (4) as shown in table 3.2**.** As the annealing temperature increase, the lattice parameters of synthesized ZnONPs were increased, i.e.an expansion of lattice parameters occurs when annealing temperature increases. Lattice parameters of synthesized nanoparticles had good agreement with that of pure zinc oxide reported by JCPDS card no. 36-1451 (a=b= 0.325 nm and c= 0.521 nm). In addition, the constant value (c/a) of synthesized nanoparticles confirms that annealing temperatures make noticeable deformation in the lattice constant [38]. Annealing temperature leads an improvement in crystal size, diffraction intensity, Zn-O bond length and unit cell volume.

Table 3.2. Lattice parameter, spacing distance, unit cell volume and bond length of synthesized ZnONPs at annealing temperatures of 700°C, 800°C and 900°C.

Annealing temperature	hkl	Lattice parameter			d_{hkl}/nm	V(A)^{03}	L(A^0)
		a(nm)	c(nm)	c/a			
700°C	101	0.2913	0.4742	1.627	0.1762	35.00	1.7821
800°C	101	0.2954	0.4756	1.617	0.1764	35.94	1.7856
900°C	101	0.2978	0.4764	1.599	0.1767	36.60	1.7894

Spherical shape and uniformly distributed zinc oxide nanoparticles were observed from scanning electron microscopy results. As shown in Fig. 3.2(a, b &c), the average size of synthesized ZnONPs was increasing with increasing annealing temperatures. An agglomeration of synthesized ZnO nanoparticles occurred during annealing temperatures was due to high surface energy of nanoparticles [39].
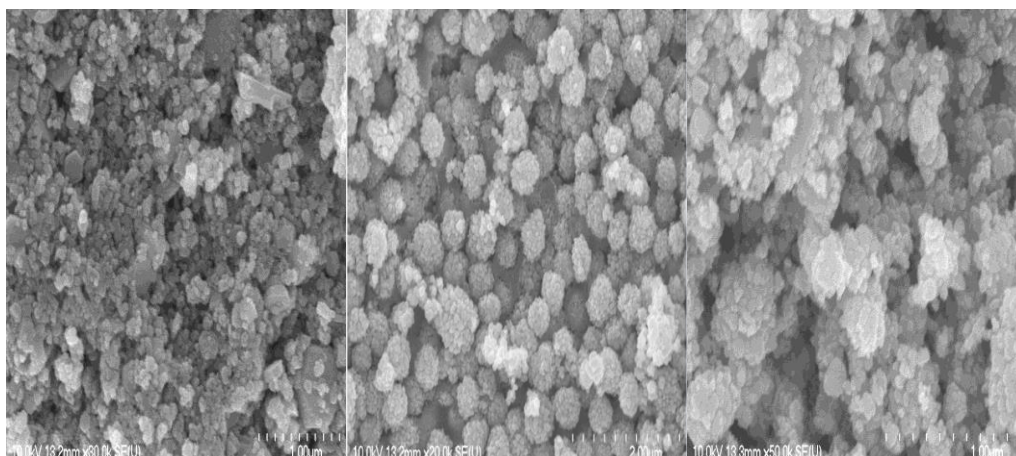
Fig. 3.2.Scanning Electron Microscope (SEM) images of synthesized ZnONPs at annealing temperature of (a) 700°C, (b) 800°C and (c) 900°C.

Fig. 3.3 shows FT-IR spectral analysis of synthesized ZnONPs in the wave number regions of 400-400cm^{-1} at annealing temperature of 700°C, 800°C and 900°C. By the process of spectroscopic characterizations, the structural and chemical compositions of ZnONPs were improved by thermal treatment. The FT-IR results of synthesized ZnONPs show that, three broadband frequency at wave number of 496, 1432, 3446cm^{-1}, 444, 1449, 3449cm^{-1} and 435, 1450 and 3425 cm^{-1} at 700°C, 800°C and 900°C of annealing temperatures respectively. The strong peaks observed in 496, 444 and 435cm^{-1} was attributed due to characteristics of the wurtzite structure of ZnONPs [39, 40]. In addition, the transmission peaks observed at around 1432, 1449 and 1450cm-1 was due to characteristics of O-H bending vibration mode of absorption of moisture [41]. Moreover, the broad transmission peaks observed in 3446, 3453 and 3449 cm-1 were due O-H stretching, vibration mode, probably due to atmospheric moisture absorbed on the surface of zinc oxide nanoparticles [42]. The FT-IR transmission peaks were increased and shifted with increasing of annealing temperature corresponding to the improved quality of the hexagonal wurtzite structure of ZnONPs [41-43].
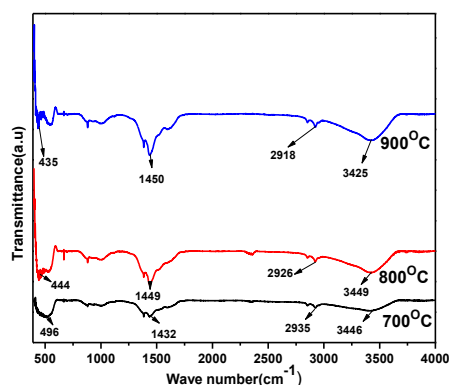
Fig. 3.3. FT-IR spectra of synthesized ZnONPs at annealing temperature of 700°C, 800°C and 900°C.

Fig. 3.4 shows typical UV/visible spectra of synthesized ZnONPs at different annealing temperature (700°C, 800°C and 900°C). The absorbance spectra of annealed ZnONPs were observed from the UV/visible spectrophotometer at room temperature in the range of 250nm-500nm and gives information about excitonic and inter transition nanoparticles. The absorption peaks were observed at 370nm, 380nm and 389nm from annealing temperature of 700°C, 800°C

and 900°C respectively. As the temperature increased, the peak absorbance wavelength was shifted from 370nm to 389nm is due to size difference [44]. The shifting in peaks was attributed to the transition of electrons from valence band to the conduction band [40-44]. The band gap energy of ZnONPs calculated using equation (6) were found to be 3.36, 3.32 and 3.27eV for annealing temperature of 700°C, 800°C and 900°C respectively. The energy band gaps of ZnONPs were decreased with increasing annealed temperature.
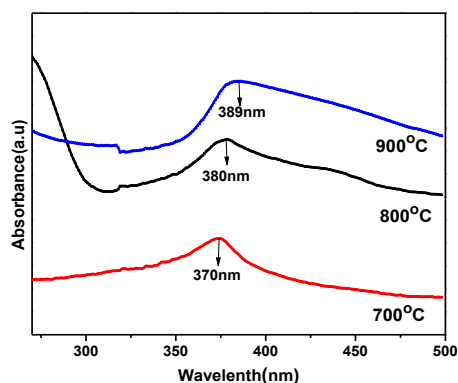
Fig. 3.4. UV/Visible Spectra of synthesized ZnONPs at annealing temperature of 700°C, 800°C and 900°C.

Fig. 3.5 shows, the emission spectra of synthesized ZnONPs at annealing temperatures of 700°C, 800°C and 900°C. The emission spectra of ZnONPs consist of two emission bands: one in the UV-region near 360nm - 400 nm and the other broadband in the visible regions (400nm-700 nm). Our samples, exhibited emission peaks at 394 nm, broad peaks at 470nm (violet region) at the annealing temperature of 700°C. Other peaks were observed at 397nm and 466 nm (blue-region) at 800°Cof annealing temperature. Additionally, the emission peaks of synthesized ZnONPs were observed at 426nm at annealing temperature of 900 ℃ (violet-region). The recombination of electron between valence band (hole) and conduction band (electrons) of synthesized NPs was attributed in UV region. The violet emission observed 426nm is ascribed to an electron transition from a shallow donor level of neutral Zni to the top level of the valance band [35]. The blue emission centered on 466 nm is attributed to singly ionized V_{Zn}. [41]. A blue green emission centered at 470 nm is due to radiative transition of electron from the shallow donor level of Z_{ni} to an acceptor level of neutral V_{zn} [42] The green emission which is not recorded in our sample is attributed to radiative transition from conduction band to the edge of the acceptor level of O_{Zn} caused by oxygen antisites (O_{Zn})[35]. The peak emissions of synthesized ZnONPs were independent of the temperature, but the emission intensity of synthesized ZnO NPs was temperature dependent [44].
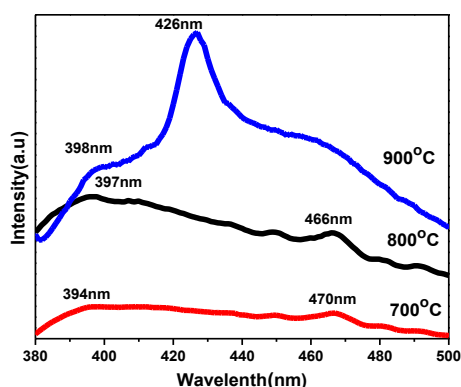
Fig. 3.5.Photoluminescence emission spectra of synthesized ZnONPs at annealing temperature of 700°C, 800°C and 900°C.

4. Conclusions

Zinc oxide nanoparticles were synthesized by sol-gel methods at annealing temperatures of 700°C, 800°C and 800°C. The prepared ZnONPs were characterized by XRD, SEM, UV/Visible Spectroscopy and Photoluminescence. The XRD revealed that synthesized nanoparticles were in the region of nanoscale (30nm-50nm) and increases as annealing temperature increased. The hexagonal wurtzite structures of synthesized ZnONPs were also confirmed from XRD results. The reduction in the FWHM and strain size with increasing temperatures has improved in crystallinity of the synthesized nanoparticles. Uniformly distributed and spherical shapes of ZnONPs were observed from SEM results.

From the FT-IR studies, with increasing annealing temperature, the presence of functional groups impurities was reduced as the particle size increased. Red shift in UV/Visible spectra of synthesized ZnONPs were observed by raising annealing temperatures. The origin of red -shift had been attributed to increase size effects and absorption intensity is increased. The emission spectra of synthesized ZnONPs showed two peaks in ultra-violet and visible regions. The emission peaks of synthesized ZnONPs were temperature independent while, but the emission intensity was temperature dependent.

References

[1] Li Li, Liu Chun-Yan, J Phys Chem **114**, 1444 (2010).
[2] Chuan-Pei Lee, Chou Chen-Yu, Chen Chia-Yuan, Yeh Min-Hsin, Lin Lu-Yin, R. Vittal et al., J Power Sources, 246 (2014).
[3] K. P. Raj, K. Sadayandi, Physica B Cond Matt **487**, 1 (2016).
[4] S. Y. Mendiola-Alvarez, J. L. Guzmán-Mar, G. Turnes-Palomino, F. Maya-Alejandro, A. Hernández-Ramírez, L. Hinojosa-Reyes, Environ Sci Pollut Res., 10 (2016).
[5] A. N. Mallika, A. R. Reddy, K. V. Reddy, J Adv ceram **4**, 123 (2015).
[6] I. Janotka, T. Nurnbergerova, Nucl Eng and Design 235, 2019 (2005).
[7] A. A. Reinert, C. Payne, L. Wang, J. Ciston, Y. Zhu, P. G. Khalifah, Inorg chem **52**, 8389 (2013).
[8] J. Lang, Q. Zhang, Q. Han, Mat Chem Phys **194**, 29 (2017).
[9] I. M. Chung, A. A. Rahuman, S. Marimuthu, A. V. Kirthi, K. Anbarasan et al., Nanomat **5**, 1317 (2015).
[10] L. Zhou, L. Wei, Y. Yang, X. Xia, P. Wang, J. Yu et al., Chem Phys **475**, 1 (2016).
[11] K. Yadav, Y. Dwivedi, N. Jaggi, J M Sci: Matter Electronics **26**, 2198 (2015).
[12] N. Bala, S. Saha, M. Chakraborty, M. Maiti, S. Das, R. Basu, P. Nandy, RSC Adv **5**(5), 4993 (2015).
[13] F. M. Mohammadi, N. Ghasemi, J Nanostruct Chem **8**, 93 (2018).
[14] Chuan-Pei Lee, Chou Chen-Yu, Chen Chia-Yuan, Yeh Min-Hsin, Lin Lu-Yin, R. Vittal et al., J Power Sources 246 (2014).
[15] V. V. Gopal, S. Kamila, Appl Nanosci **7**, 75 (2017).
[16] M. Goswami, N. C. Adhikary, S. Bhattacharjee, Optik 158, 1006 (2018).
[17] A. Belay, B. Bekele, A. R. Chandra Reddy, DJNB **14**, 140 (2019).
[18] N. F. Jaafar, A. M. M. Najman, A. Marfur, N. W. C. Jusoh, J Photochemy and Photobiol A Chem **388**, 112202 (2020).
[19] D. Leila, L. G. Mar, B. Fatima, N. Abddelyamine, B. Ali, H. Nacereddine, J Theoret and Appl

Phys **12**, 159 (2018).

[20] A. M. Holi, A. A. Al-Zahrani, A. S. Najm, P. Chelvanathan, N. Amin, Chem Phys Lett **59**, 137486 (2020).

[21] N. Kataria, V. K. Garg, M. Jain, K. Kadirvelu, Adv Powder Techn **27**, 1180 (2016).

[22] J. Lang, Q. Zhang, Q. Han, Y. Fang, J. Wang et al., Mater Chem and Phys **194**, 29 (2017).

[23] T. A. Feiona, G. Sabeena, M. S. Bagavathy, E. Pushpalaksmi, J. J. Samra, G. Annadurai, J Appl Sci Env Manag **24**, 1079 (2020).

[24] H. H. Basri, R. A. Talib, R. Sukor, S. H. Othman, H. Ariffin, Nanomat **10**, 1061 (2020).

[25] A. K. Zak, M. E. Abrishami, M. W. H. Abd et al., Ceram Intern **37**, 393 (2011).

[26] L. Jurablu, S. Farahmandjou, T. P. Firoozabadi, J Sci **26**, 281 (2015).

[27] M. Kahouli, A. Barhoumi, A. Bouzid, A. Al-Hajry, S. Guermazi, Superlatt Microstruct **85**, 7 (2015).

[28] N. M. A. Hadia, S. García-Granda, J. R. Garcia, J Nanosci and Nanotechn **14**, 5443 (2014).

[29] H. R. Ghorbani, F. P. Mehr, H. Pazoki, B. M. Rahmani, Orie J Chem **31**, 1219 (2015).

[30] I. M. Alibe, K. A. Matori, E. Saion, A. M. Ali, M. H. M. Zaid, Sci Sintering, 49 (2017).

[31] M. B. Mohamed, Intern J Appl Ceram Techn **17**, 823 (2020).

[32] P. B. Taunk, R. Das, D. P. Bisen, R. K. Tamrakar, J Rad Resear Appl Sci **8**, 433 (2015).

[33] A. K. Zak, W. A. Majid, M. E. Abrishami, R. Yousefi, Soli Stat Sci **13**, 251 (2011).

[34] T. M. Hammad, J. K. Salem, R. G. Harrison, J Superlatt Microstr **47**, 335 (2010).

[35] S. Alireza, M. Monsen, G. Mansour, J Luminesc **3**, 229 (2009).

[36] M. Kooti, A. N. Sedeh, J Chem 2013.

[37] M. S. Ghamsari, S. Alamdari, D. Razzaghi, M. A. Pirlar, J Luminesc **205**, 508 (20196).

[38] D. Verma, A. K. Kole, P. Kumbhakar, J Alloy Comp **625**, 122 (2015).

[39] A. N. Mallika, A. R. Reddy, K. V. Reddy, J Adv Ceram **4**, 123 (2015).

[40] R. Davood, Rene Ener Syst **50**, 932 (2013).

[41] N. V. Kaneva, C. D. Dushkin, Bulg Chem Commun **43**, 259 (2011).

[42] N. A. Salahuddin, M. E. Kemary, E. M. Ibrahim, J Nanosci Nanotechn **5**, 82 (2015).

[43] Y. Wang, C. Zhang, S. Bi, G. Luo, Powder Techn **202**(1), 130 (2010).